Geomechanics and Engineering, *Vol. 17, No. 4 (2019) 393-403*
DOI: https://doi.org/10.12989/gae.2019.17.4.393

Experimental research on dynamic response of red sandstone soil under impact loads

Tong Wang[1,2], Zhanping Song*[1,3], Jianyong Yang[2a], Junbao Wang[1,3b] and Xuegang Zhang[1]

[1]School of Civil Engineering, Xi'an University of Architecture and Technology, Xi'an 710055, China
[2]School of Resources and Environmental Engineering, Jiangxi University of Science and Technology, Ganzhou 341000, China
[3]Shaanxi Key Laboratory of Geotechnical and Underground Space Engineering, Xi'an 710055, China

(Received September 18, 2018, Revised February 4, 2019, Accepted March 6, 2019)

Abstract. The cycling impact test of red sandstone soil under different axial pressure and different impact loads are conducted to reveal the mechanical properties and energy consumption mechanism of red sandstone soil with static-dynamic coupling loading. The results show that: Under the action of different axial pressure and different impact loads, the peak stress of the specimen increases, and then tends to be stable with the times of impact. With the increase of impact times, the specific energy absorption value of the red sandstone soil specimen is increased first and then gentle development trend. When the impact loads are certain, the larger the axial pressure is, the smaller the peak value of energy absorption, which indicates that the energy utilization rate is not high under the condition of large axial pressure. Through the analysis of energy utilization, it is found that the smaller the impact load, the higher the energy utilization rate. The greater the axial pressure, the lower the energy utilization rate. when the axial pressure is large, the impact loads corresponding to the maximum values of reflectivity, transmissivity and absorptivity are the same. The relationship between reflectivity and transmissivity is negatively correlated.

Keywords: red sandstone soil; static-dynamic coupling loading; stress-strain; specific energy absorption value; energy utilization rate

1. Introduction

In 1991, the International Conference on the Development and Utilization of Underground Space was held in Tokyo, Japan. At the meeting, scholars from countries around the world have reached a consensus that the 19th century is the century of bridges, the 20th century is the century of high-rise building, while the 21st century will be the century of underground space utilization (Kishii 2016, Cheng *et al.* 2018). During the construction of underground engineering, the soil is inevitably affected by the dynamic load (impact loads), such as the subway tunnel construction (Mishra *et al*. 2018, Song *et al*. 2016, Wang *et al*. 2017), the earthquake (Cheng *et al*. 2014, Kawamata *et al.* 2016), and the engineering blasting (Jayasinghe *et al.* 2017, Li *et al.* 2018), which may leads to the redistribution of soil stress field and brings about adverse effects. Therefore, studies on the mechanical behavior and energy consumption mechanism of the soil under dynamic loading have great significance to the underground engineering construction.

In recent years, relevant scholars have made great research about the dynamic mechanical response of geomaterials under impact loads. Song *et al*. (2009) obtained the dynamic compression stress-strain curve and the quasi-static compression performance of dry sand by using the improved Split Hopkinson Pressure Bar and the MTS810 material testing system. Analyzed the effect of strain rate on its compression response under static-dynamic loading, found that the initial density and the lateral confinement level have a greater influence on the compression response than loading condition. Luo *et al.* (2011) improved the traditional Split Hopkinson Pressure Bar to research the dynamic compression behavior and the relationship between energy absorption and compressibility of dry sand under high strain rate and compression stress, the experimental results indicated that there is a power law between the stress-strain and initial volume density, and the index is 8.25. Jin *et al.* (2013) used the static-dynamic loading test unit to study the impact resistance ability of sandstone under cycle loading with different axial pressure and confining pressure, and found the impact resistance ability increases as the axial pressure decreases or the confining pressure increases. Li *et al.* (2014) explored the influence of length and diameter ratio to the energy dissipation of red sandstone, the results showed that the energy dissipation ratio decreases with the increase of length and diameter ratio during the red sandstone failure process. Hong *et al.* (2009) researched the energy dissipation characteristics of sandstone, limestone and granite under impact loading by using the SHPB device, the results suggested that the energy dissipation density and the dynamic strength of rock exhibit logarithmic relation. Liu *et*

*Corresponding author, Professor
E-mail: songzhpyt@xauat.edu.cn
[a]Professor
E-mail: xgjy123@163.com
[b]Professor
E-mail: xajdwangjunbao@163.com

http://www.techno-press.org/?journal=gae&subpage=7
ISSN: 2005-307X (Print), 2092-6219 (Online)

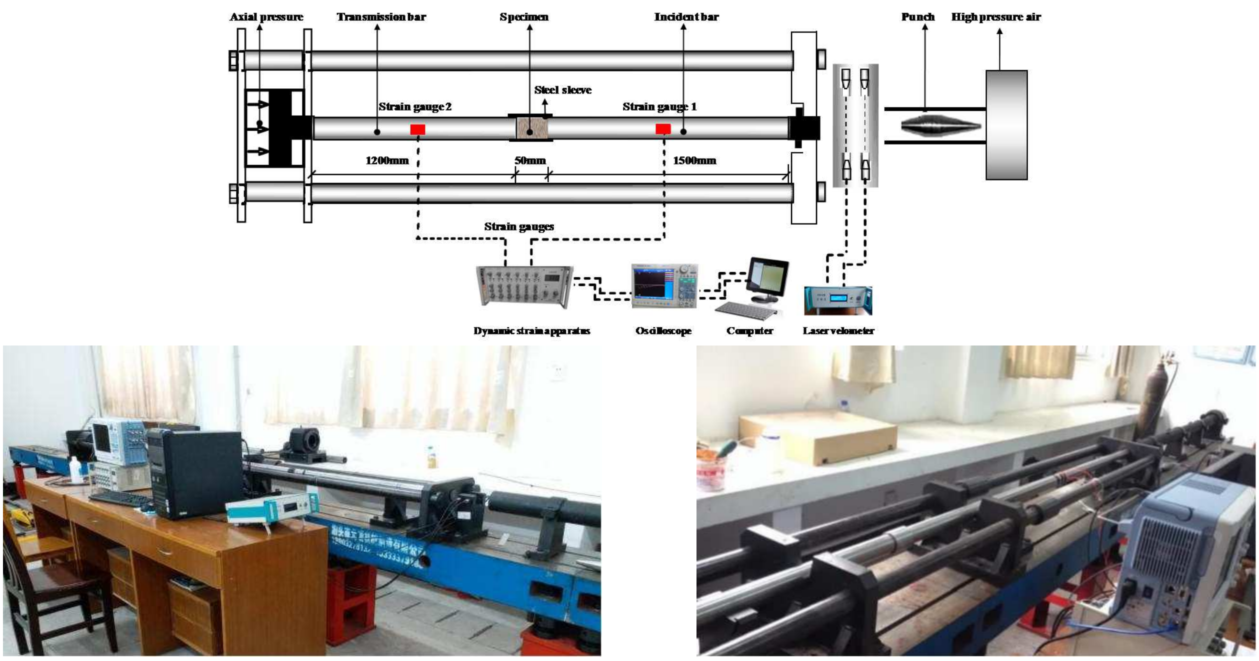

Fig. 1 Modified Split Hopkinson pressure bar testing system

al. (2015) used the MTS hydraulic servo control test machine and Split Hopkinson Pressure Bar to study the failure mode, fracture strength and energy dissipation characteristics of coal rock under quasi-static and dynamic compression conditions, which provides an important reference for coal mining.

When studying the mechanical properties of soil under dynamic load, for soil with less than 1m buried depth, which crustal stress is small and can be ignored, just consider the effect of dynamic load. While for soil with more than 10m, the crustal stress can't be neglected, in this condition, the soil is under the effect of static-dynamic load (Nikadat *et al*. 2016, Ranjbarnia *et al*. 2016). Therefore, the effect of coupled static-dynamic load should be considered while studying the mechanical behavior of deep soil under dynamic load. However, the objectives of previous studies on the mechanical properties and energy dissipation mechanism under coupled static-dynamic load were rock (Chakraborty *et al*. 2016, Kim *et al.* 2018, Huang *et al*. 2017), rather than soil (Omidvar *et al*. 2012, Yang *et al.* 2017, Li *et al.* 2018). To research the dynamic mechanical properties and energy consumption mechanism of red sandstone soil subjected to impact loads, a series of tests under different axial compression and different impact loads are carried out by using the improved SHPB test device. This paper provides a reference for the stability of red sandstone soil foundation and the stability analysis of tunnel surrounding rock.

2. Experiments

2.1 Experiment apparatus

The experiment was completed in the laboratory of Jiangxi University of Science and Technology, the improved Split Hopkinson Pressure Bar (Fig. 1) mainly includes four parts, the power system consists of a high-pressure nitrogen cylinder and a chamber, the load and energy transfer system consists of a punch, an incident bar (1500 mm×50 mm), a transmission bar (1200 mm×50 mm) and a soil specimen (50 mm×50 mm) (Hill 1950, Davies and Hunter 1963) in steel sleeve, the speed measuring system consists of a laser velometer and the strain test system consists of a strain gauge, a dynamic strain apparatus and an oscilloscope. During the experiment, the impact loads were adjusted by controlling the pressure of the high pressure gas chamber (high pressure nitrogen) to realize the constant speed impact load. The axial pressure was adjusted by controlling the axial pressure loading device of a manual oil pump to realize the constant axial pressure.

2.2 Equipment principle

The SHPB test technique bases on two basic assumptions, uniformity assumption and first-order assumption. According to the measured incident wave ε_I, reflected wave ε_R and transmitted wave ε_T, combined with one-dimensional stress wave theory, the strain rate, strain and stress of geomaterial material can be calculated.

$$\begin{cases} \dot{\varepsilon}(\mathrm{t}) = -\dfrac{2\,\mathrm{C_e}}{L}\varepsilon_R \\ \varepsilon(\mathrm{t}) = -\dfrac{2\,\mathrm{C_e}}{L}\displaystyle\int_0^L \varepsilon_R dt \\ \sigma(\mathrm{t}) = -\dfrac{A_\mathrm{e}}{A_s}E_e\varepsilon_T \end{cases} \tag{1}$$

Assuming that the stress wave energy is W, according to the energy balance principle and the integral principle, the

Table 1 The physical and mechanical properties of the red sandstone soil

Dry density /g·cm^{-3}	Moisture content/%	Liquid limit/%	Plastic limit/%	Cohesion /kPa	Internal friction angle / °
1.88	7.5	25.5	9.3	19.68	34.61

energy balance equation of the material is obtained.

$$W = \frac{A_e}{\rho_e C_e}\int_0^{\tau}\sigma^2(t)dt, C_e^2\rho = E_e \tag{2}$$

$$\begin{cases} W_I(t) = \dfrac{A_e}{\rho_e C_e}\displaystyle\int_0^{\tau}\sigma_I{}^2(t)dt \\ W_R(t) = \dfrac{A_e}{\rho_e C_e}\displaystyle\int_0^{\tau}\sigma_R{}^2(t)dt \\ W_T(t) = \dfrac{A_e}{\rho_e C_e}\displaystyle\int_0^{\tau}\sigma_T{}^2(t)dt \end{cases} \tag{3}$$

where: A_e is the cross section area of the elastic bar, E_e is the elastic modulus of the alloy bar, t is the duration of the stress wave, $\rho_e C_e$ is the wave impedance of the elastic bar, L is the length of the specimen, A_s is the cross section area of the specimen.

2.3 Specimen preparation

The red sandstone soil used in the experiment, which has uniform particle sizes and mainly concentrates in the range of 2~5 mm, were taken from Ganzhou City, Jiangxi, Province, China (east longitude 113°54'-116°38', northern latitude 24°29'-27°09'). The physical and mechanical properties of the red sandstone soil are shown in Table 1.

The specimen preparation process is as follows: (1) according to the dry density and moisture content of the specimen, the required dry soil mass and moisture content were calculated and stirred it fully then put it in a plastic bag for 12 hours to prevent moisture loss and ensure even distribution of moisture in the specimen. (2) butter was applied to the inner wall of the casing, and put the prepared specimen into the steel sleeve, which can be effectively reduced the friction between the red sandstone soil and the pipe wall. The coupling of stress wave at the "bar-soil" interface is guaranteed, and the experimental error is reduced. (3) the specimen was prepared according to the Standard for soil test method. It was compacted in three layers by stratification method, the height of each drop hammer remained unchanged, each layer was compacted 10 times and subjected to nap treatment to prevent delamination of the specimen. the specimen size of 50mm x 50mm was prepared. Due to the height of the hitting hammer and the falling hammer used for preparing the specimen was small, the impact load used to prepare the sample was far less than the impact load of the experiment itself, so the initial behavior of the sample under cyclic impact load can be neglected. In order to ensure that the soil specimen in the casing is completely in contact with the two-bar interface, the parallelism of the last layer of the specimen must be strictly ensured with an error of less than±0.05 mm to ensure uniform transmission of the axial impact force. There are 16 specimens were prepared in this experiment.

2.4 Experiment schemes and procedures

In order to study the influence of axial pressure and impact loads on the mechanical properties and energy dissipation of red sandstone soil, the impact test under different axial pressure and different impact loads were carried out by means of dynamic and static combined loading. In the test, four axial pressure conditions were sequentially set to 0 MPa, 9 MPa, 18 MPa and 27 MPa, the impact loads of 0.25 MPa, 0.50 MPa, 0.75 MPa and 1.00 MPa were sequentially applied under each axial pressure condition. When the axial pressure was 0 MPa, there were 8 cyclic impacts under different impact loads. When the axial pressure was 9 MPa, 18 MPa and 27 MPa, there were 6 cyclic impacts under different impact loads.

The experiment process consists of the following steps: (1) Before the experiment, air flush the static and dynamic combined loading device to check whether the strain gauges are available and whether the incident bar and the transmission bar were in good contact. If all was well, the specimen shall be installed. (2) Install the specimen, in order to ensure good contact between the two bar and specimen, appropriate butter should be applied on the contact surface of the incident bar, transmission bar and specimen, the specimen of the casing should be clamped between the two bar. (3) After the installation of the specimen, adjust the manual oil pump so that the meter value was the experimental set value (0 MPa, 9 MPa, 18 MPa, 27 MPa), adjust the depth of the bullet in the chamber to about 97mm, and adjust the air pressure to the experimental set value (0.25 MPa, 0.50 MPa, 0.75 MPa, 1.00 MPa) to ensure that the incident energy was approximately equal during the cyclic impact process. (4) At the beginning of the experiment, when the axial pressure was 0 MPa, there were 8 cyclic impacts under different impact loads. When the axial pressure was 9 MPa, 18 MPa and 27 MPa, there were 6 cyclic impacts under different impact loads. At the end of each impact, the value of the oil pressure gauge should be checked to prevent the problem of axial pressure caused by the compression of soil due to the impact, and appropriate supplementary pressure should be carried out to maintain the axial pressure at the set value of the experiment.

3. Mechanical properties analysis based on the principle of SHPB test

3.1 Characteristics of the stress wave shape curve

Fig. 2 shows the waveform of the specimen under the impact load of 0.25 MPa without axial pressure when striking the 1~8 times. As shown in Fig. 2, the stress wave waveform of the red sandstone changed obviously during cyclic impact. The incident wave waveform collected in the

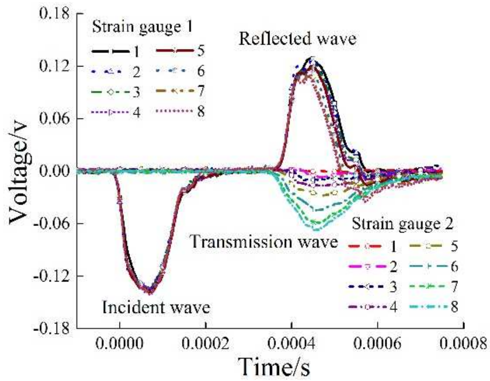

Fig. 2 Waveform diagram of the specimen under the same impact velocity

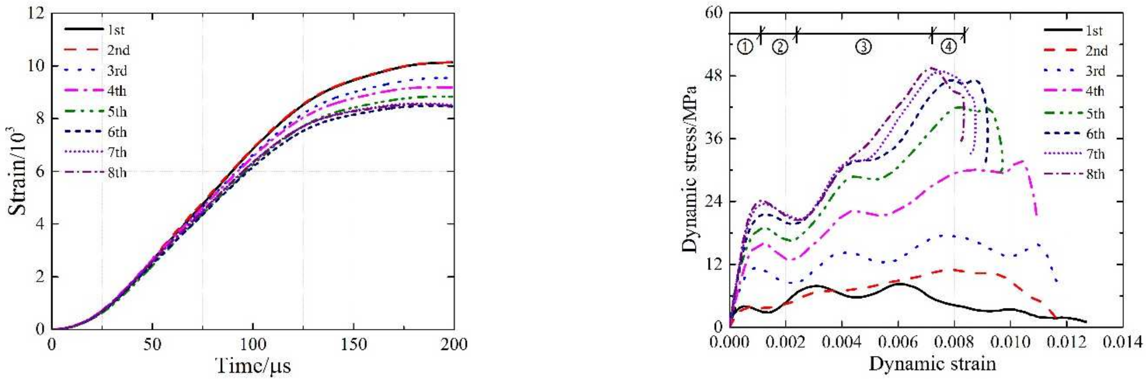

(a) Dynamic time-strain curves of the specimen without axial pressure

(b) Dynamic stress-strain curves of the specimen without axial pressure

Fig. 3 Characteristics of the stress-strain curves

experiment indicates that the incident waves are basically coincident, which means all impact test have the same incident energy. While the transmission amplitude increases with impact times by the size of the transmission wave crest, the peak of reflected wave decreases with the increase of the impact times, and the phenomenon of “double peaks” of reflected wave appears, This is mainly due to the large difference in wave impedance between the specimen and the bar, which makes the stress wave generated by the impact can be transmitted to the transmission bar less through the specimen, and most of it is reflected to the incident bar. For certain red sandstone soil specimen with invariant incident energy, the internal porosity of the specimen commonly expressed by the transmittance. From this knowable, the porosity of the specimen decreases and the transmission increases gradually with the increasing of impact times, which means the specimen structure tends to dense under the impact loads.

3.2 Characteristics of the stress-strain curves

Fig. 3(a) shows the dynamic time-strain curve of the specimen without axial pressure. As can be seen from Fig. 3(a), with the increase of impact times, the strain gradually decreases and the shape variable also gradually decreases, the specimen is compressed gradually and the internal pores are gradually reduced. In addition, the time-history curves of the initial and later stages of cyclic impact basically coincide, which indicates that the physical properties of the specimen do not change much under the small impact load at the initial stage of the experiment. However, with the increase of impact times, the specimen gradually compacted, and in the later stage of the experiment, the specimen has reached a certain degree of compactness, which results in the time history curves of 7 and 8 times of cyclic impact once again coincide.

Fig. 3(b) shows the dynamic stress-strain curve of the specimen under impact load of 0.25 MPa without axial pressure when striking the 1~8 times. From Fig. 3(b), it can be seen that in the initial stage of the impact, there is a large number of pores inside the specimen, and the energy produced by the impact is mainly converted into the slip between the soil particles, the collapse of the pores and the rearrangement of the particles. The porosity of the specimen decreases gradually and the stress begins to rise with the increase of the cumulative impact times, the distribution is dispersed in the whole graphics area, the stress growth amplitude is uniform. When the specimen reaches a certain degree of compactness (taking the 8th cyclic impact as an example), the stress-strain curves of the specimen can be divided into four stages: ①sharp rise stage, ②descending stage, ③slow ascending stage, ④sharp decline stage. ①Sharp rise stage: during the initiation of loading, a large increase in stress occurs, and this stage approximately considered as an elastic stage. The compactness of the specimen increases while the stress first time reaches the

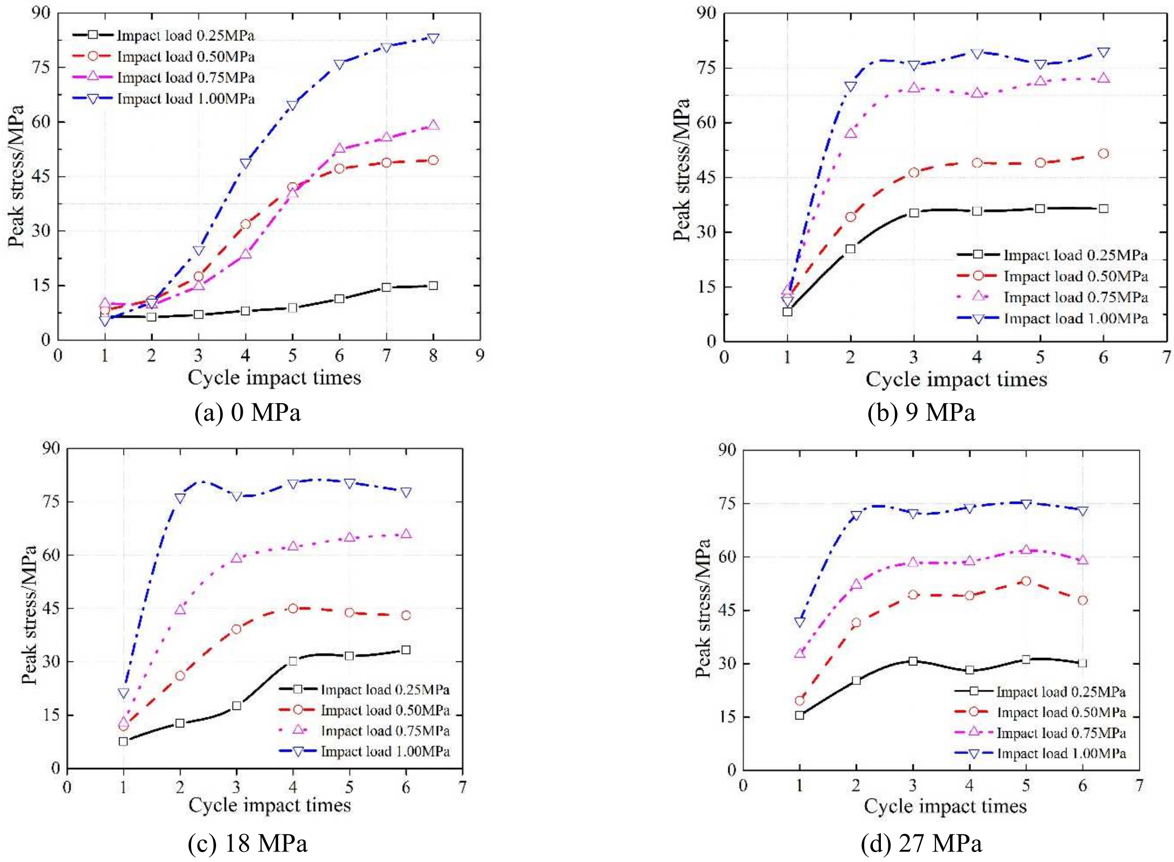

(a) 0 MPa (b) 9 MPa

(c) 18 MPa (d) 27 MPa

Fig. 4 Relationship between peak stress and impact times

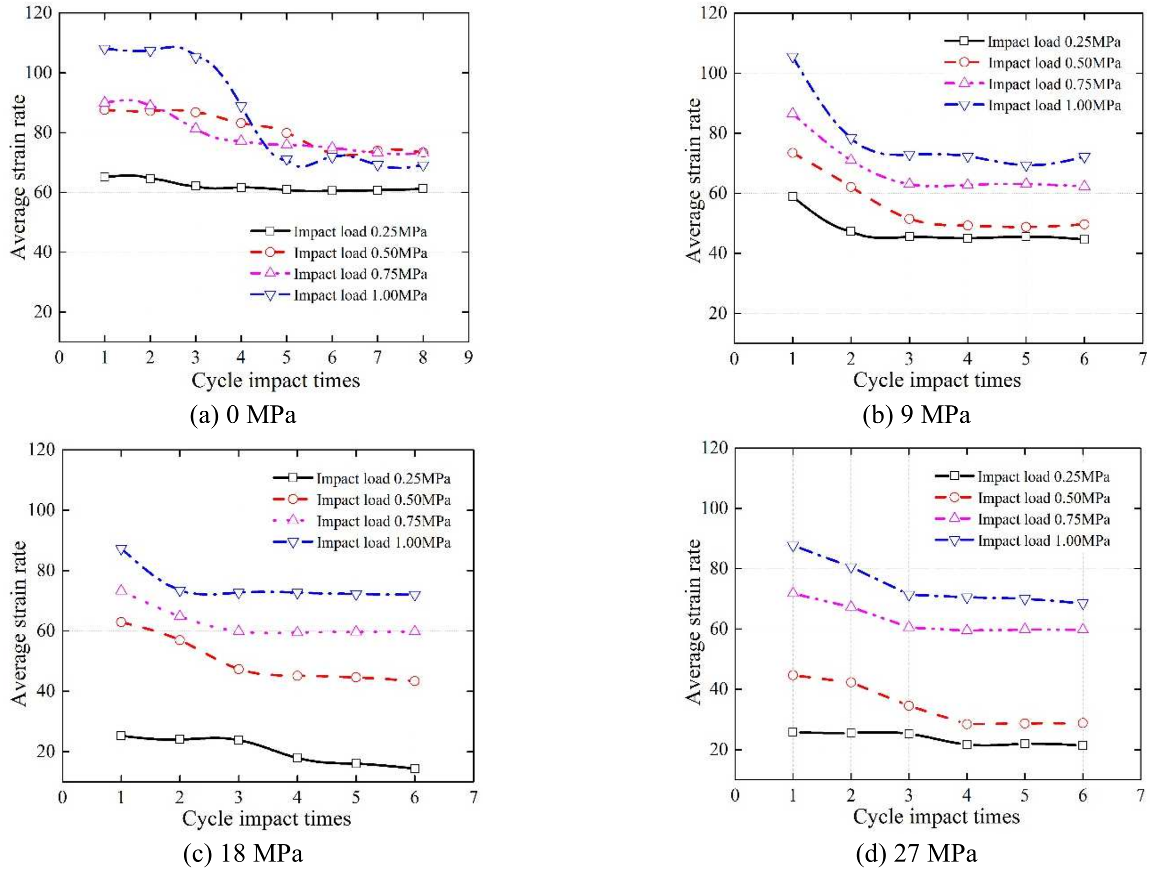

(a) 0 MPa (b) 9 MPa

(c) 18 MPa (d) 27 MPa

Fig. 5 Relationship between average strain rate and impact times peak value. ②Descending stage: due to the too rapid loading rate, there exists a force lag effect, which leads to the dynamic stress of the specimen decreases. ③Slow ascending stage: when the specimen is in full force state, the compactness of the specimen increases with the increase of stress. And stress gradient increases with the increase of the cumulative impact until the reaches the peak stress of the loading interval. ④Sharp decline stage: when the stress reaches a certain value, the stress begins to drop sharply, indicating that the specimen becomes denser with impact loads. The stress rises sharply while the strain increase amplitude decreases. During the whole loading process, the third stage costs the most of the time, and the specimen deformation is the largest, the compaction effect is the best in this stage.

3.3 Characteristics of peak stress variation

Fig. 4 shows the relationship between peak stress and impact times of the specimen under different axial pressure and different impact loads. From Fig. 4, the peak stress of the specimen increases gradually with the impact times, and finally tends to be stable.

By comparing the peak stress curves of the specimen under different axial pressure and different impact loads show that the axial pressure and impact loads have a great influence on the peak stress of the specimen. Fig. 4(a) shows that as the impact times increase, the amplitude of peak stress is positively associated with the impact loads under the condition of no axial pressure. There are three stages: slow growth, sharp growth and steady development. Figs. 4(b)-(d) indicate that when there exists axial pressure, with the increase of impact times, the larger impact loads, the larger peak stress value. There are two stages: sharp growth and steady development. This is because the specimen is subjected to the three-dimension effect, namely, casing, axial pressure and impact loads. Under the greater axial pressure and impact loads, the earlier of time for the peak stress of the specimen get the largest value, the earlier enters the steady stage. In addition, it can be found that no matter how the axial pressure and the impact load change, the peak stress will reach a certain value and no longer increase with the impact times, the specimen has a certain degree of density.

3.4 Characteristics of average strain rate variation

Fig. 5 shows the relationship between average strain rate and impact times of the specimen. It can be seen from Fig. 5 that average strain rate of the specimen decreases with the increase of impact times under different impact loads of the same axial pressure, and finally tends to steady development.

By comparing the relationship between the average strain rate and the impact times under different conditions, it can be seen that with the increase of the impact times, the average strain rate of the specimen decreases gradually. As a whole, the larger impact load, the greater difference between the initial and stationary values of the average strain rate. The larger the axial pressure, the smaller initial value and final value of the average strain rate. Fig. 5(a) shows that the average strain rate decreases gradually with the increase of impact times without axial pressure, the change of the average strain rate is the greatest when the impact load is 1 MPa. Figs. 5(b)-5(d) shows that the larger impact loads, the greater difference between the initial and stationary values of the average strain rate. Under the same impact load, the difference between the average strain rate at the last impact and the average strain rate at the previous impact gradually decreases with the increase of impact times, and the final difference tends to zero. From the relationship between the average strain rate and the reflection wave in Eq. (1) shows that the reflection wave decreases with the decreasing of the average strain rate. At the same time, combining the relationship between incident wave, reflected wave and transmitted wave: $\sigma_I(t)=\sigma_R(t)+\sigma_T(t)$, it can be seen that under the same incident energy, the reflection wave decreases gradually and the transmittance increases, which indicates that the inner pore of the specimen decreases gradually and the specimen is getting stronger.

4. Energy dissipation analysis based on the principle of SHPB energy balance

4.1 Analysis of specific energy absorption value

In order to analyze the energy consumption mechanism of the specimen, this paper makes the following assumptions: (1) No energy loss in the elastic bar and the section of the specimen. (2) The kinetic energy of the special-shaped punch completely translate into the energy carried by the incident wave. Based on the law of conservation of energy, the energy absorbed by the deformation of the specimen is related to the energy carried by the incident wave, the reflection wave, and the transmission wave, which can be calculated by the following formula.

$$W_A(\mathrm{t}) = W_I(t) - W_R(t) - W_T(t) \tag{4}$$

$$W_A(t) = \frac{A_e}{\rho_e C_e}\int_0^{\tau}\left[\sigma_I^{\,2}(t) - \sigma_R^{\,2}(t) - \sigma_T^{\,2}(t)\right]dt \tag{5}$$

where: $W_A(t)$-absorption energy, $W_I(t)$-Incident energy, $W_R(t)$-reflection energy, $W_T(t)$-transmission energy.

Under the impact loads, the energy consumed in the process of compaction can be considered in terms of the energy dissipation capacity of the specimen in addition to the measurement of energy absorbed. Therefore, the unit volume absorption energy of red sandstone soil is introduced, that is the specific energy absorption value W_v.

$$W_V(t) = \frac{W_A(t)}{A_s L} \tag{6}$$

where: A_s -specimen cross-section area, L -specimen initial length.

When the axial pressure is 18 MPa, the incident energy,

Table 2 The partial date of specimen under different impact loads with axial pressure of 18 MPa

Impact load /MPa	Impact times /Time	$W_I(t)$/J	$W_R(t)$/J	$W_T(t)$/J	η_R /%	η_T/%	η_A/%
	1	30.79	26.96	2.83	87.56	9.18	3.26
	2	31.62	21.50	7.34	67.99	23.23	8.78
0.25	3	33.84	19.05	10.63	56.29	31.41	12.3
	4	34.30	16.96	13.51	49.45	39.4	11.15
	5	31.00	11.50	15.70	37.08	50.64	12.28
	6	30.16	9.05	17.32	30.00	57.41	12.59
	1	41.70	39.60	1.70	94.97	4.09	0.94
	2	43.42	29.49	7.03	67.91	16.18	15.91
0.50	3	41.70	22.97	12.20	55.08	29.27	15.65
	4	42.78	20.39	16.14	47.65	37.72	14.63
	5	41.92	18.39	17.38	43.86	41.46	14.68
	6	41.64	15.38	19.98	36.93	47.98	15.09
	1	75.61	71.10	3.36	94.04	4.45	1.51
	2	77.72	51.63	18.05	66.42	23.22	10.36
0.75	3	72.35	39.40	25.69	54.45	35.51	10.04
	4	75.43	37.74	30.57	50.03	40.53	9.44
	5	77.56	36.94	33.44	47.63	43.12	9.25
	6	78.23	35.86	35.26	45.83	45.07	9.10
	1	100.03	89.47	4.90	89.44	4.89	5.67
	2	99.26	47.54	41.58	47.90	41.89	10.21
1.00	3	99.75	46.48	43.91	46.60	44.03	9.37
	4	99.60	46.21	44.72	46.40	44.90	8.70
	5	100.46	45.43	46.29	45.22	46.08	8.70
	6	99.71	44.01	46.80	44.14	46.93	8.93

reflection energy and transmission energy of the specimen under different impact loads are shown in Table 2. Therefore, the specific energy absorption value of the specimen can be calculated by the Eq. (6).

Fig. 6 shows the relationship between the specific energy absorption value and the impact times of the specimen. From Fig. 6, it is found that with the increases of impact times, the specific energy absorption value of the specimen increases first and then develop smoothly. Fig. 6(a) shows that when the axial pressure is 0 MPa, the specific energy absorption value increases with the increase of impact times with a small growth rate, and when the impact times reach a certain value, the specific energy absorption value tends to stabilize. While the impact load is 0.75 and 1.00 MPa, the change law of the specific energy absorption value is basically consistent. Therefore, under the condition of no axial compression, the specific energy absorption value does not increase with the impact load when the impact load is greater than 0.75 MPa. Fig. 6(b)-6(d) indicates that with the increase of the impact times, the specific energy absorption value increases more rapidly than the condition of no axial pressure is applied, and only a few impact times (3-4 times) results in the specific energy absorption tends to be stable, and the larger the impact load, the greater the peak value of the specific energy absorption value. Compared with the different axial pressure, when the axial pressure is 27 MPa, the peak value of the specific energy absorption decreased, which indicates that excessive axial pressure goes against the energy absorption.

4.2 Analysis of energy utilization rate

The impact loading process is the process of compacting by air pressure on red sandstone soil specimen. The absorption energy of the specimen is determined by the energy of the incident wave, the reflection wave and the transmission wave, and the absorbed energy is mainly used for the slip, friction and rearrangement of the soil particles in the specimen, so that the inner pores of the soil are closed and the soil is compacted. The energy utilization rate of the specimen during impact can be calculated by the following formula.

$$w = \frac{W_A(t)}{W_I(t)} \times 100\% \tag{7}$$

Under the condition of 0 MPa and 9 MPa axial pressure, the energy utilization rate of the red sandstone soil specimen is calculated by the Eq. (7), and the relationship between energy utilization efficiency and impact times can be obtained.

Fig. 7 shows the change of energy utilization efficiency with impacts times. As can be seen from Fig. 7(a), with $N \leq 6$ impact times, the energy utilization rate increases with the impact times. The energy utilization rate is the highest when the impact times reaches 6 times, and the impact load is smaller, the energy utilization rate is higher. This is because there is a lot of porosity inside the specimen, and the energy transfer requires a certain time and process. When the impact load is small, the energy generated by the impact is mainly converted into the slip between the soil particles, the collapse of the pores and the rearrangement of the particles, the pores gradually decrease and the energy utilization rate is higher. When the impact load is large, the instantaneous production of larger impact energy, so that the water inside the specimen cannot be discharged in time, and the pressure is assumed together with the solid particles to form the resistance mechanism, at this time the energy utilization rate is relatively small. With $6<N<8$ impact times, energy utilization rate does not increase with the number of impacts, and the curve is flat and basically tends to stabilize. As can be seen from Fig. 7(b), when the axial pressure is 9 MPa, the change trend of energy utilization rate is increased first then decreased slightly and flat development finally. With the increase of impact times, the energy utilization rate rises sharply. The impact load of 0.25 MPa, 0.50 MPa, 0.75 MPa and 1.00 MPa reached the peak of energy utilization rate at the 4th, 2nd, 2nd and 2nd impacts respectively. The energy utilization rate of the specimen of red sandstone soil decreased slightly after reaching the peak value, because the loading rate of the specimen is too fast, which results in the lag effect and decrease of the energy utilization rate of the specimen. Increasing the number of impacts again, the energy utilization rate basically stabilized. As can be seen from

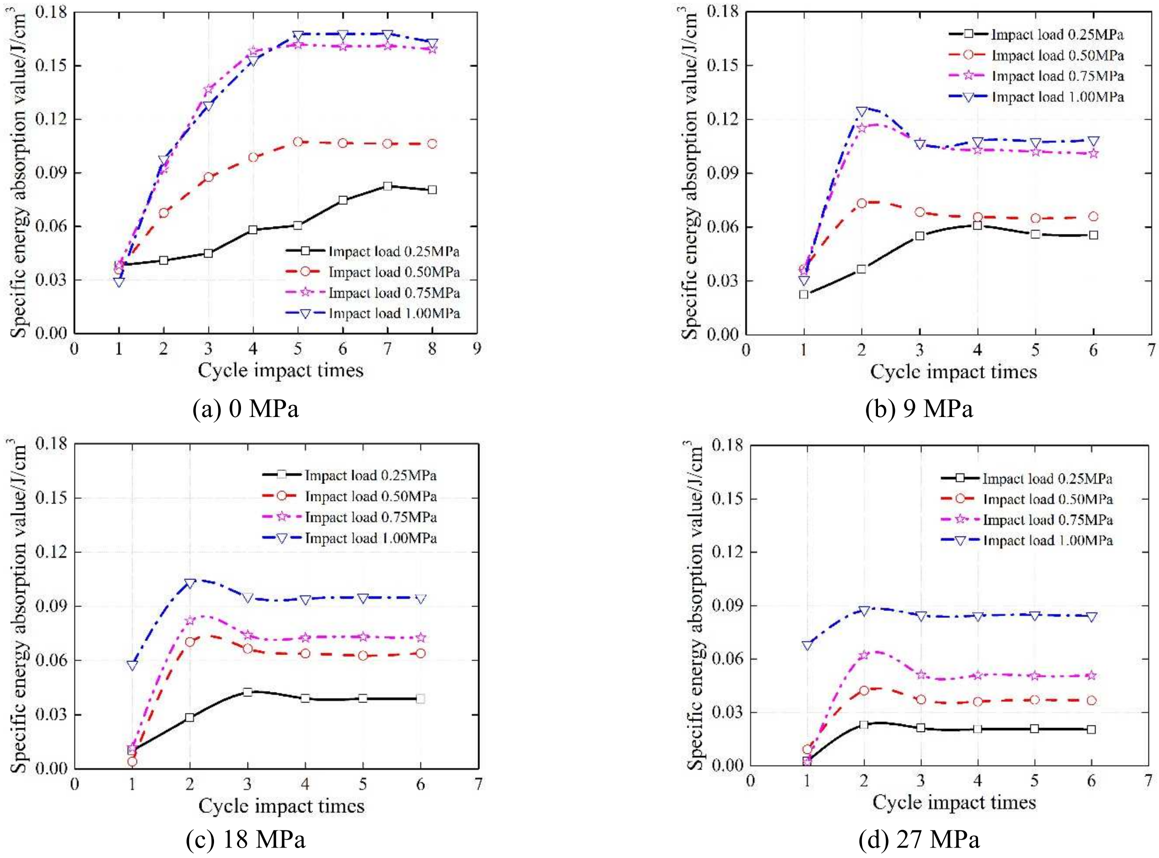

Fig. 6 The change of specific energy absorption value with impact times

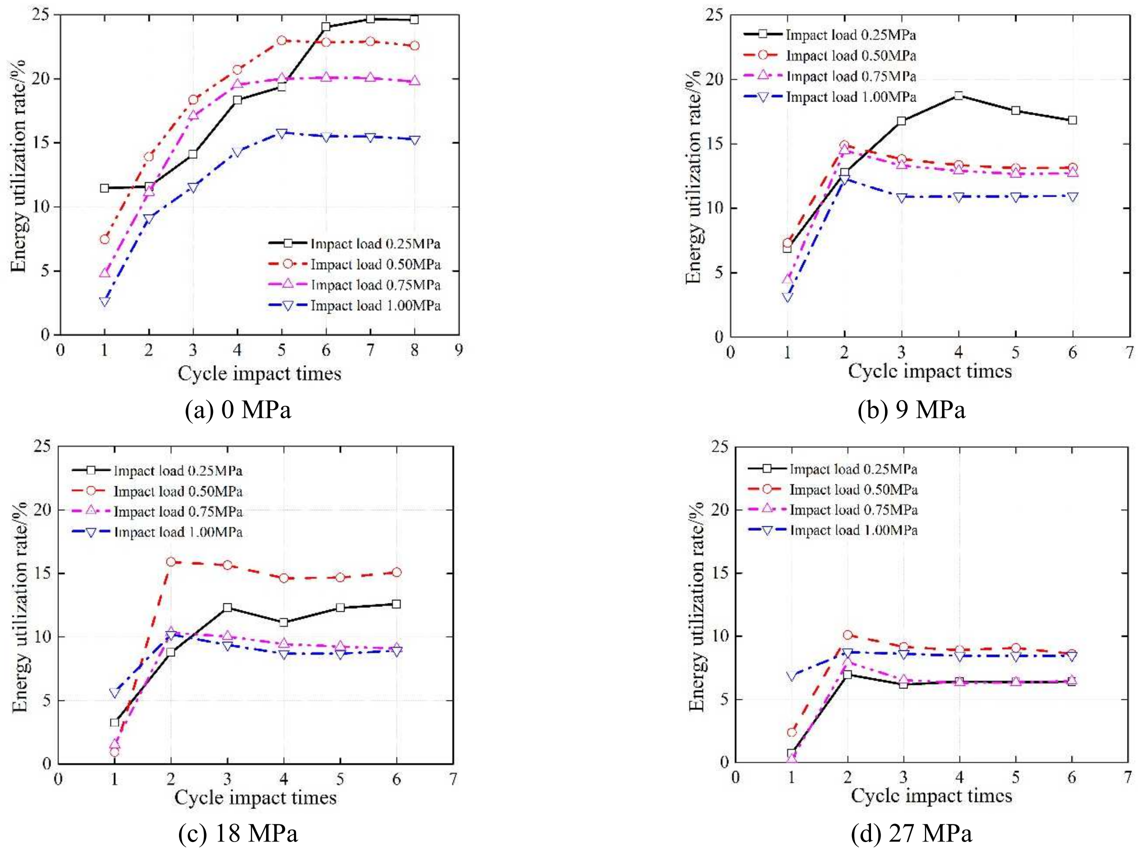

Fig. 7 The change of energy utilization rate with impact times

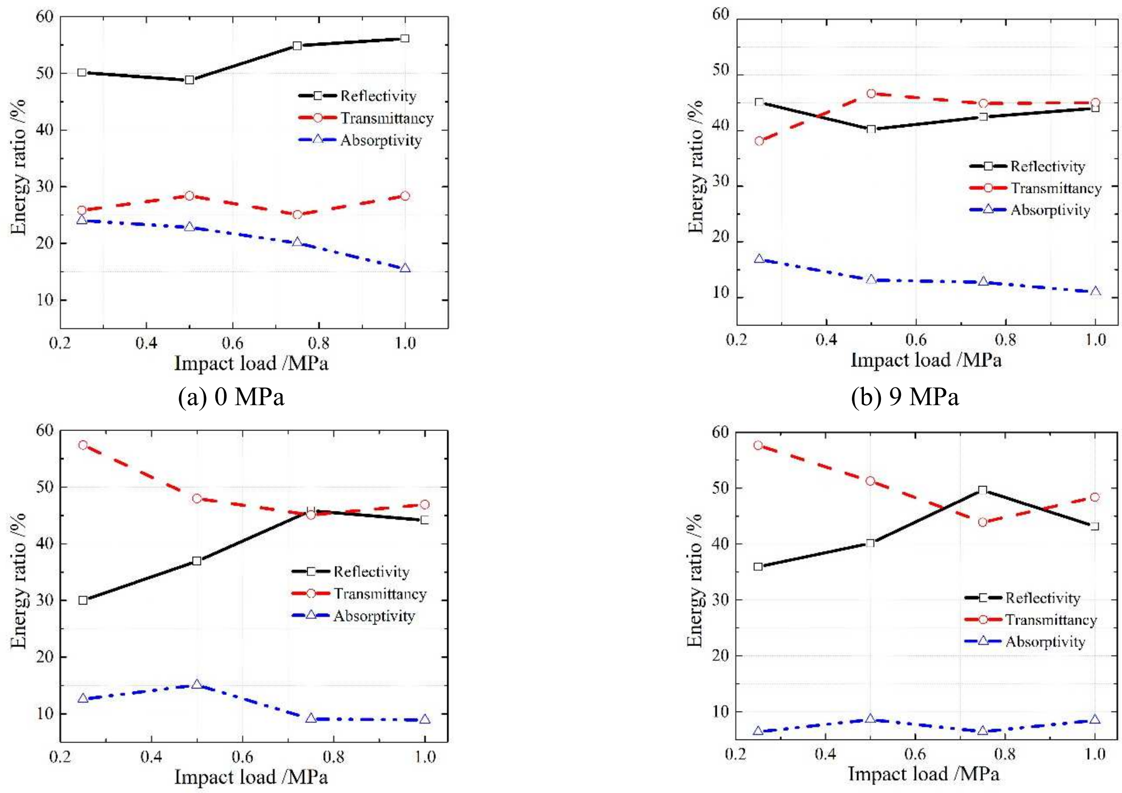

(a) 0 MPa (b) 9 MPa

(c) 18 MPa (d) 27 MPa

Fig. 8 The change of energy ratio with impact loads

Figs. 7(c) and 7(d), with the increase of impact loads, the change trend of energy utilization rate is increased first then decreased slightly and flat development finally, and there is a maximum value. When the axial pressure is 18 MPa, the impact load of 0.25 MPa, 0.50 MPa, 0.75 MPa and 1.00 MPa reached the peak of energy utilization rate at the 3rd, 2nd, 2nd and 2nd impacts respectively. When the axial pressure is 27 MPa, with the increase of impact loads, the maximum energy utilization rate is reached at the second cyclic impact.

To sum up, with no axial pressure, when the impact times reaches about 6 times, the energy utilization efficiency is the highest, the impact load is 0.25 MPa, 0.5 MPa, 0.75 MPa, 1.00 MPa, the corresponding energy utilization rate peak is 24%, 22%, 20% and 15% respectively. When axial pressure is 9 MPa, the impact load is 0.25 MPa, 0.5 MPa, 0.75 MPa, 1.00 MPa, the corresponding energy utilization rate peak is 19%, 14%, 14% and 12% respectively. Compared with the 0 MPa and 9 MPa data, it is found that the smaller the impact load, the higher the energy utilization rate. The greater the axial pressure, the lower the energy utilization rate.

When axial pressure is 18 MPa, the impact load is 0.25 MPa, 0.5 MPa, 0.75 MPa, 1 MPa, the corresponding energy utilization rate peak is 12%, 16%, 10% and 10% respectively. When axial pressure is 27 MPa, the impact load is 0.25 MPa, 0.5 MPa, 0.75 MPa, 1.00 MPa, the corresponding energy utilization rate peak is 7%, 10%, 8% and 9% respectively. Compared with the 18 MPa and 27 MPa data, it is found that the change rule of energy utilization rate is not obviously related to the impact loads with the increase of impact times under large axial pressure.

4.3 Analysis of energy ratio

According to Eq. (4), the energy reflectivity, transmissivity and absorptivity of the specimen can be expressed as follows

$$\eta_R = \frac{W_R}{W_\mathrm{I}} \times 100\% \tag{8}$$

$$\eta_T = \frac{W_T}{W_I} \times 100\% \tag{9}$$

$$\eta_A = \frac{W_A}{W_I} \times 100\% \tag{10}$$

where: η_R-reflectivity, η_T-transmissivity, η_A -absorptivity.

According to the Eqs. (8)-(10), the reflectivity, transmissivity and absorptivity of the specimen can be calculated with the test data.

Fig. 8 shows the variation of reflectivity, transmissivity and absorptivity with the impact loads at 6th times the cumulative impact. It is shown from Fig. 8 that when there is no axial pressure, the reflectivity decreases first and then increases, the transmissivity keeps fluctuating up and down in a certain range, the absorptivity of energy decreases gradually. The impact loads corresponding to the maximum values of reflectivity, transmissivity and absorptivity are 1.00 MPa, 0.5 MPa, 0.25 MPa, respectively. When the axial pressure is 9 MPa, the reflectivity decreases first and then increases, the transmissivity increases first and then decreases, however, the absorptivity of energy in general decreases. The impact loads corresponding to the maximum values of reflectivity, transmissivity and absorptivity are 0.25 MPa, 0.5 MPa, 0.25 MPa, respectively. When the axial pressure is 18 MPa, the reflectivity and absorptivity of energy are both increases first and then decreases, the transmissivity decreases first and then increases, The impact loads corresponding to the maximum values of reflectivity, transmissivity and absorptivity are 0.75 MPa, 0.25 MPa, 0.50 MPa, respectively. When the axial pressure is 27 MPa, the reflectivity increases first and then decreases, the transmissivity decreases first and then increases, the absorptivity keeps fluctuating up and down in a certain range, The impact loads corresponding to the maximum values of reflectivity, transmissivity and absorptivity are 0.75 MPa, 0.25 MPa, 0.50 MPa, respectively.

In summary, it can be seen that when the axial pressure is 18 MPa and 27 MPa, the impact loads corresponding to the maximum values of reflectivity, transmissivity and absorptivity are the same. When the axial pressure is 0 MPa and 9 MPa, the impact loads corresponding to the maximum values of transmissivity and absorptivity are the same. With the increase of axial pressure, the absorptivity decreases gradually, indicating that the excessive axial pressure is not conducive to the absorption of energy. The relationship between reflectivity and transmissivity is negatively correlated, which is consistent with the variation rule of Eq. (4).

5. Conclusions

This paper takes red sandstone soil as the research object, the dynamic response characteristics of red sandstone soil with cyclic impact under the confined conditions. The influences of different axial pressure and different impact loads on the dynamic mechanical properties and energy dissipation mechanism of red sandstone soil are revealed.

The conclusions are as follows:

• According to the test results, the dynamic stress-strain curve of the red sandstone soil specimen can be divided into four stages: sharp rise stage, descending stage, slow ascending stage and sharp decline stage. Sharp rise stage: At the initial stage of loading, the stress rises sharply. The red sandstone soil deformation is the largest in the slow ascending stage of the stress, and the compaction effect is the best.

• Under the action of different axial pressure and different impact loads, the peak stress of the red sandstone soil specimen increases, and then tends to be stable with the times of impact.

• With the increase of impact times, the specific energy absorption value of the red sandstone soil specimen is increased first and then gentle development trend. When the impact loads are certain, the larger the axial pressure is, the smaller the peak value of energy absorption, which indicates that the energy utilization rate is not high under the condition of large axial pressure.

• When the axial pressure is large, the impact loads corresponding to the maximum values of reflectivity, transmissivity and absorptivity are the same. The relationship between reflectivity and transmissivity is negatively correlated.

The results can provide a theoretical basis for the mechanical properties and energy dissipation law of red sandstone soil under impact loads at different depths. Especially for the application of roadbed filling, subway tunnel excavation, compaction of deep pile foundation of the super high-rise building, backfilling of goaf in the deep coal mine, etc., the dynamic response characteristics under the accidental load encountered in the construction process and later use process are explored. However, this experiment only focuses on the preliminary study of the dynamic mechanical properties of small specimens, and the applied axial pressure has a large range, which has certain limitations on its practical application. In the later research, we will further improve it to make it more research significance and practical value.

Acknowledgements

The authors deeply appreciate support from the National Natural Science Foundation(51578447) and the Ministry of housing and urban construction science and technology project (2017-k4-032).

References

Chakraborty, T., Mishra, S., Loukus, J., Halonen, B. and Bekkala, B. (2016), "Characterization of three himalayan rocks using a split hopkinson pressure bar", *Int. J. Rock Mech. Min. Sci.*, **85**, 112-118.

Cheng, W.C., Song, Z.P., Tian, W. and Wang, Z.F. (2018), "Shield tunnel uplift and deformation characterisation: A case study from Zhengzhou metro", *Tunn. Undergr. Sp. Technol.*, **79**, 83-95.

Cheng, X.S., Xu, W.W., Yue, C.Q., Du, X.L. and Dowding, C.H. (2014), "Seismic response of fluid-structure interaction of undersea tunnel during bidirectional earthquake", *Ocean Eng.*, **75**(1), 64-70.

Davies, E.D.H. and Hunter, S.C. (1963), "The dynamic compression testing of solidsbythe method of the split hopkinson bar", *Mech. Phys. Solids*, **11**(3), 155-179

Hill, R. (1950), *The Mathematical Theory of Plasticity*, Oxford University Press, New York, U.S.A.

Hong, L., Zhou, Z.L., Yin, T.B., Liao, G.Y. and Ye, Z.Y. (2009), "Energy consumption in rock fragmentation at intermediate strain rate", *J. Central South Univ.*, **16**(4), 677-682.

Huang, M., Xu, C.S., Zhan, J.W. and Wang, J.B. (2017), "Comparative study on dynamic properties of argillaceous siltstone and its grouting-reinforced body", *Geomech. Eng.*, **13**(2), 333-352.

Jayasinghe, L.B., Zhou, H.Y., Goh, A.T.C., Zhao, Z.Y. and Gui, Y.L. (2017), "Pile response subjected to rock blasting induced ground vibration near soil-rock interface", *Comput. Geotech.*, **82**, 1-15.

Jin, J.F., Li, X.B. and Zhong, H.B. (2013), "Study of dynamic mechanical characteristic of sandstone subjected to three-dimensional coupled static-cyclic impact loadings", *Chin. J.*

Rock Mech. *Eng*., **32**(7), 1358-1372.
Kawamata, Y., Nakayama, M., Towhata, I. and Yasuda, S. (2016), “Dynamic behaviors of underground structures in e-defense shaking experiments”, *Soil Dyn*. *Earthq*. *Eng*., **82**, 24-39.
Kim, E., Garcia, A. and Changani, H. (2018), “Fragmentation and energy absorption characteristics of red, berea and buff sandstones based on different loading rates and water contents”, *Geomech*. *Eng*., **14**(2), 151-159.
Kishii, T. (2016), “Utilization of underground space in Japan”, *Tunn*. *Undergr*. *Sp*. *Technol*. *Incorp*. *Trenchless Technol*. *Res*., **55**, 320-323.
Li, D.W. and Fan, J.H. (2018), “A study of mechanical property of artificial frozen clay under dynamic load”, *Adv*. *Civ*. *Eng*., 1-8.
Li, M., Mao, X.B., Lu, A.H., Tao, J., Zhang, G.H., Zhang, L.Y. and Li, C. (2014), “Effect of specimen size on energy dissipation characteristics of red sandstone under high strain rate”, *Int*. *J*. *Min*. *Sci*. *Technol*., **24**(2), 151-156.
Li, X.B., Li, C.J., Cao, W.Z. and Tao, M. (2018), “Dynamic stress concentration and energy evolution of deep-buried tunnels under blasting loads”, *Int*. *J*. *Rock Mech*. *Min*. *Sci*., **104**, 131-146.
Liu, X.H., Dai, F., Zhang, R. and Liu, J.F. (2015), “Static and dynamic uniaxial compression tests on coal rock considering the bedding directivity”, *Environ*. *Earth Sci*., **73**(10), 5933-5949.
Luo, H., Lu, H., Cooper, W.L. and Komanduri, R. (2011), “Effect of mass density on the compressive behavior of dry sand under confinement at high strain rates”, *Exper*. *Mech*., **51**(9), 1499-1510.
Mishra, S., Rao, K.S., Gupta, N.K. and Kumar, A. (2018), “Damage to shallow tunnels in different geomaterials under static and dynamic loading”, *Thin-Walled Struct*., **126**, 138-149.
Nikadat, N. and Marji, M.F. (2016), “Analysis of stress distribution around tunnels by hybridized fsm and ddm considering the influences of joints parameters”, *Geomech*. *Eng*., **11**(2), 269-288.
Omidvar, M., Iskander, M. and Bless, S. (2012), “Stress-strain behavior of sand at high strain rates”, *Int*. *J*. *Impact Eng*., **49**(2), 192-213.
Ranjbarnia, M., Oreste, P., Fahimifar, A. and Arya, A. (2016), “Analytical-numerical solution for stress distribution around tunnel reinforced by radial fully grouted rockbolts”, *Int*. *J*. *Numer*. *Anal*. *Meth*. *Geomech*., **40**(13), 1844-1862.
Song, B., Chen, W.N. and Luk, V. (2009), “Impact compressive response of dry sand”, *Mech*. *Mater*., **41**(6), 777-785.
Song, Z.P., Yang, T.T. and Jiang, A.N. (2016), “Elastic-plastic numerical analysis of tunnel stability based on the closest point projection method considering the effect of water pressure”, *Math*. *Prob*. *Eng*., 1-12.
Wang, J.B., Song, Z.P., Zhao, B.Y., Liu, X.R., Liu, J. and Lai, J.X. (2017), “A study on the mechanical behavior and statistical damage constitutive model of sandstone”, *Arab*. *J*. *Sci*. *Eng*., **43**(10), 5179-5192.
Yang, R.S., Chen, J., Yang, L.Y., Fang, S.Z. and Liu, J. (2017), “An experimental study of high strain-rate properties of clay under high consolidation stress”, *Soil Dyn*. *Earthq*. *Eng*., **92**, 46-51.

IC